Crumbs2 Promotes Cell Ingression During the Epithelial-to-Mesenchymal Transition at Gastrulation

Nitya Ramkumar[1,2], Tatiana Omelchenko[3], Nancy F. Silva-Gagliardi[4], C. Jane McGlade[4], Jan Wijnholds[5] and Kathryn V. Anderson[1]

1. Developmental Biology Program, Sloan Kettering Institute, Memorial Sloan Kettering Cancer Center, 1275 York Avenue, New York, New York 10065, USA

2. Program in Biochemistry and Structural Biology, Cell and Developmental Biology, and Molecular Biology, Weill Cornell Graduate School of Medical Sciences, Cornell University, 1300 York Avenue, New York, New York 10065, USA

3. Cell Biology Program, Sloan Kettering Institute, Memorial Sloan Kettering Cancer Center, 1275 York Avenue, New York, New York 10065, USA

4. The Hospital for Sick Children, Arthur and Sonia Labatt Brain Tumor Research Center and Department of Medical Biophysics, University of Toronto, Toronto, Ontario M5G 1X8, Canada

5. Department of Ophthalmology, Leiden University Medical Center, 2333 ZA Leiden, The Netherlands

Correspondence should be addressed to KVA, k-anderson@ski.mskcc.org

Abstract

During gastrulation of the mouse embryo, individual cells ingress in an apparently stochastic pattern during the epithelial-to-mesenchymal transition (EMT). Here we define a critical role of the apical protein Crumbs2 (CRB2) in the gastrulation EMT. Static and live imaging show that ingressing cells in *Crumbs2* mutant embryos become trapped at the primitive streak, where they continue to express the epiblast transcription factor SOX2 and retain thin E-cadherin-containing connections to the epiblast surface that trap them at the streak. CRB2 is distributed in a complex anisotropic pattern on apical cell edges, and the level of CRB2 on a cell edge is inversely correlated with the level of Myosin IIB. The data suggest that the distributions of CRB2 and Myosin IIB define which cells will ingress and we propose that cells with high apical CRB2 are basally extruded from the epiblast by neighboring cells with high levels of apical myosin.

An epithelial to mesenchymal transition (EMT) during gastrulation establishes the three layers of the animal body plan (ectoderm, mesoderm and endoderm) through a defined sequence of morphological transformations[1,2,3,4]. Defects in the gastrulation EMT and in subsequent mesoderm migration are a significant cause of human birth defects[5]. EMTs are also required for formation of many organs and are associated with tumor progression[6,7].

Gastrulation of amniotes (e.g. birds and mammals) requires a sequence of coordinated cellular events. The gastrulation EMT begins with the breakdown of the basement membrane underlying the epithelial epiblast at a single position, the primitive streak, which marks the future posterior pole of the body plan. Basement membrane breakdown is rapidly followed by apical constriction and a basal shift of the nucleus of an ingressing epiblast cell, followed by dissolution of apical tight and adherens junctions, and, finally, acquisition of a migratory program in cells of the nascent mesoderm and definitive endoderm. This EMT is triggered by a convergence of secreted signals (Wnt, Nodal, FGF, BMP)[8] and is coupled to changes in transcription factor expression, including loss of expression of the pluripotency-associated factor SOX2 and upregulation of the mesenchymal factor SNAIL1[9].

The amniote primitive streak is a dynamic cell population: as cells leave the primitive streak epithelium to populate the mesoderm, they are continuously replaced by cells from the adjacent epiblast epithelium. It is not known how the stable morphology of the primitive streak is maintained despite this continuous flux[4]. Cells at the chick or mouse primitive streak exit from the epiblast epithelium as individuals, while the adjacent cells of the epiblast retain their apical junctions[3,4]. Thus amniote gastrulation, like collective cell migration, requires dynamic neighbor exchanges while simultaneously maintaining the integrity of the epithelium.

Here we show that mouse Crumbs2 (CRB2) promotes cell ingression during gastrulation. In contrast to the best-defined role of *Drosophila* Crumbs protein as a determinant of the apical domain of epithelial cells[10,11], epithelial polarity is normal in the epiblast of *Crumbs2* mutants, but cells of the late (>E7.5) primitive streak fail to delaminate and remain tethered to the apical surface of the epiblast epithelium by thin E-cadherin-containing connections. Thus mouse CRB2 is required to remove, rather than maintain, apical junctions. We also find that CRB2 is localized in a complex anisotropic pattern in cells of the epiblast. Localized CRB2 accumulation is inversely correlated with the level of apical Myosin IIB, consistent with the hypothesis that CRB2

is an essential component of a system that directs stochastic actomyosin-dependent cell ingression during gastrulation.

Results

CRB2 is required for normal mesoderm production

Mammals have three members of the Crumbs family. Mutations in human or mouse *Crumbs1* cause light-dependent retinal degeneration but do not affect viability[12]. Mice lacking *Crumbs3* survive to birth with defects in lung and intestinal epithelia[13]. Mouse *Crumbs2* mutants initiate post-implantation development normally but arrest at mid-gestation (~E9.0) with a syndrome of morphological defects, including a deficit of mesoderm and an abnormal neural plate[14,15]. Both *Crumbs2* RNA and protein are expressed in the epiblast, but not the endoderm or mesoderm layers, of the E6.75 and E7.5 embryo (Supplementary Fig. 1).

To test whether CRB2 overlaps in function with other Crumbs family proteins, we analyzed the phenotypes of double and triple mutant embryos. *Crumbs2*$^{-/-}$ *Crumbs3*$^{-/-}$ and *Crumbs1*$^{rd8/rd8}$ *Crumbs2*$^{-/-}$ double mutant embryos and *Crumbs1*$^{rd8/rd8}$ *Crumbs2*$^{-/-}$ *Crumbs3*$^{-/-}$ triple mutant embryos all expressed the primitive streak marker *Brachyury* (*T*) in the normal posterior domain at E7.5, had reduced paraxial mesoderm, marked by *Meox1* expression, and an abnormal neural plate at E8.5 (Fig. 1A, B), indicating that only CRB2 has a critical role in the early embryo.

Although Crumbs is required for establishment of the apical domain of epithelia in the *Drosophila* embryo, markers of apical-basal polarity were correctly localized in the epiblast of E7.75 *Crumbs2*$^{-/-}$ mutant and the *Crumbs2*$^{-/-}$ *Crumbs3*$^{-/-}$ double mutant embryos. ZO1, a component of tight junctions, pERM, an apical membrane marker, and the Par complex proteins aPKCλ and Par3 were apically localized in wild type and mutants (Fig. 1C). γ-tubulin+ centrosomes were apical and Arl13b+ cilia extended from the apical surface of cells of the E7.5 *Crumbs2*$^{-/-}$ *Crumbs3*$^{-/-}$ epiblast (Fig.1C).

CRB2 promotes cell ingression

The primitive streak of the mouse embryo, marked by the expression of the transcription factor Brachyury (T), is the region of the posterior epiblast where cells delaminate from the epithelium to form the mesoderm and definitive endoderm germ layers. At the early bud stage (E7.5), one

day after the initiation of gastrulation, the primitive streak regions of wild-type and *Crumbs2*$^{-/-}$ mutant embryos were similar in morphology (Fig. 1D). At this stage, cells of the wild-type epiblast epithelium expressed SOX2 and cells in the mesoderm layer expressed SNAIL1 (Fig. 1E). In E7.5 *Crumbs2*$^{-/-}$ mutants, the width of the streak, as defined by the size of the break in the basement membrane, was comparable to the wild type and a thin SNAIL1+ mesoderm layer was present (Fig. 1E).

Twelve hours later, at E8.0, the primitive streak of the *Crumbs2*$^{-/-}$ mutant was dramatically engorged with cells. At this stage, many layers of SOX2-positive cells had accumulated at the primitive streak (Fig. 1F). At E8.0, the region of laminin breakdown at the mutant streak was wider than in wild type and cells expressing E-cadherin had accumulated at the streak (Supplementary Fig. 2A). Indistinguishable defects were seen in *Poglut1*^{wsnp} embryos (Fig. 1F), which lack CRB2 activity due to an independent genetic lesion: POGLUT1 is required for the glycosylation of extracellular EGF repeats, which is required for cell surface localization of CRB2 [ref. 15]. In contrast, mutants with blocked mesoderm migration, such as *Rac1*, accumulate SNAIL1-positive cells near the streak (Supplementary Fig.2B).

Scanning electron micrographs (SEMs) of E7.75 wild-type embryos showed that some epiblast cells at the streak had basally-displaced nuclei and cell protrusions, suggesting that they were acquiring mesodermal characteristics (Fig. 2A, A'). In SEMs of E7.75 *Crumbs2*$^{-/-}$ mutant embryos, some nuclei in the streak region were far from the epiblast surface but the cells remained attached to the apical surface of the epiblast by thin projections (Fig. 2B, B'). Similar defects were seen in cells at the *Poglut1*^{wsnp} streak (Fig. 2C, C').

To visualize the shapes of individual cells, we labeled individual cells with an X-linked GFP transgene that expresses cytoplasmic GFP in a mosaic manner as a result of random X-inactivation in female embryos[16]. Some apically constricted cells at the wild-type primitive streak had cell bodies displaced from the apical surface of the epiblast (Fig. 2D, G). In *Crumbs2*$^{-/-}$ and *Poglut1*^{wsnp} mutant embryos, cell bodies far from the apical surface remained attached to the apical surface of the epiblast (Fig. 2E, F, H). The thin cytoplasmic connections to the apical surface of delaminating *Crumbs2*$^{-/-}$ and *Poglut1*^{wsnp} streak cells were E-cadherin-positive (Fig. 2E, F), indicating that these cells had failed to dissolve their apical adherens junctions, a necessary step in the EMT. We infer that the SOX2+, E-cadherin+ cells that accumulated at the

mutant streak remained integrated within the epiblast epithelium, and were therefore arrested in the midst of the EMT.

Live imaging defines cell ingression dynamics

To compare the dynamics of cell ingression of wild-type and mutant streak cells, we labeled individual cells by mosaic activation of GFP expression using the EIIA-Cre, mT/mG system[3] and followed cell behavior in E7.5 cultured embryos by live confocal imaging. In the wild-type embryo, ingressing cells were apically constricted and had basal protrusions; they displaced their cell bodies basally and exited the epithelium in less than 2 hours (30-110 min; n=5 cells) (Supplementary Videos 1-3; Fig. 3A, D). In *Crumbs2*$^{-/-}$ mutants, cells at the streak constricted their apical membrane as the cell body moved basally, but they failed to leave the epithelium in the duration of imaging (>200 minutes; n=5 cells) (Supplementary Videos 4-6; Fig. 3B, D), leading to an accumulation of bottle-shaped cells with long thin apical extensions at the streak (Fig. 3C).

Autonomous and non-autonomous CRB2 activities

Consistent with the epiblast-specific expression of CRB2 (Supplementary Fig. 1), deletion of a conditional *Crumbs2* allele in epiblast-derived cells using the *Sox2-Cre* transgene[17] reproduced the deficit of paraxial and axial mesoderm seen in the null mutants (Supplementary Fig. 3), which demonstrated that CRB2 is required in embryonic rather than extraembryonic lineages. The *Brachyury (T)*-Cre becomes active in cells of the mid-to-late streak stage primitive streak (E7.5)[18]. Conditional deletion of *Crumbs2* with *T-Cre* allowed formation of somewhat more mesoderm than in *Crumbs2* null mutants (Fig 4A), but recapitulated most aspects of the null phenotype: paraxial mesoderm was reduced and SOX2+ mutant cells accumulated in the late primitive streak (Fig 4B). Thus *Crumbs2* is required specifically in the cells of the primitive streak for cell ingression and efficient production of mesoderm.

To examine cell autonomy at high resolution, we generated chimeric embryos using *Crumbs2* mutant that expressed the membrane marker GPI-GFP[19] (see Methods). After injection of GFP+ *Crumbs2*$^{-/-}$ ES cells into wild-type blastocysts, chimeric embryos were analyzed at E8.5 (Fig. 4C). High percentage chimeras (95-100% mutant cells; n=9) recapitulated the *Crumbs2*$^{-/-}$ phenotype (Supplementary Fig. 4B). In chimeric embryos with a lower contribution of mutant cells (10-40%; n=20), the overall morphology of the embryos appeared normal (Supplementary Fig. 4A) and mutant cells were incorporated into normal-appearing epithelia (Fig. 4D, E).

Although *Crumbs2*$^{-/-}$ embryos did not form clear somites, *Crumbs2* mutant cells were incorporated into somites in chimeric embryos (Fig. 4E), indicating that they had undergone both the primitive streak EMT and the mesodermal-to-epithelial transition (MET) that produces the somites.

In chimeric embryos, CRB2 was not detected on most of the edges of wild-type cells adjacent to mutant cells (GFP+) at the streak (Fig. 4F-F'') and in the neural epithelium (Supplementary Fig 4C). In the same cells, actin (Fig. 4F, 4F''') and β-catenin (Supplementary Fig 4C) localized normally at boundaries between wild-type and mutant cells, suggesting that stability of membrane CRB2 may depend on homophilic interactions with adjacent cells, as seen in *Drosophila* and zebrafish[20,21,22].

Complex spatial distribution of CRB2

CRB2 was enriched apically in the E6.75 and E7.75 epiblast (Fig. 5A, B; Supplementary Fig. 1D). At the early headfold stage (E7.75), there was a posterior-to-anterior gradient of apical CRB2, with approximately 4-fold higher levels near the streak than in the anterior epiblast (Fig 5B, B'). The posterior enrichment suggested that CRB2 has an instructive, rather than permissive, role in behavior of cells at the primitive streak.

En face imaging of the apical surface of the epiblast showed that the surface area of epiblast cells was variable, although the tight junction protein ZO1 was expressed at similar levels on all edges of epiblast cells (Fig. 5C). In contrast, CRB2 was localized in complex anisotropic patterns (Fig. 5D). The anisotropic distribution was apparent in both the epiblast layer of the streak and in the adjacent epiblast (Supplementary Fig. 5); the highest CRB2 levels were >50-fold higher than the lowest levels. The distribution of edges with high CRB2 was, in part, correlated with cell topology: nearly half of triangular cells had high CRB2 on all edges, whereas only 10-15% of cells with 5 or 6 sides had CRB2 on all edges (Supplementary Fig. 5).

PATJ (INADL), a member of the Crumbs complex[23] was also distributed anisotropically in the epiblast (Supplementary Fig. 6A), providing independent confirmation of the anisotropic localization of the Crumbs complex. Apical PATJ could not be detected in the primitive streak region of *Crumbs2*$^{-/-}$ or *Poglut1*^{wsnp} embryos (Supplementary Fig 6B), consistent with a requirement of CRB2 for PATJ localization in the early mouse embryo.

In addition to the global anisotropic distribution of CRB2, there was strong punctate CRB2 staining in the region of the primitive streak (Fig. 5D, E). Transverse sections of embryos in which individual cells expressed the X-linked GFP transgene showed that the strong CRB2 puncta corresponded to the apical membranes of highly constricted primitive streak cells (Fig. 5E, E'), suggesting that apically constricted cells that are poised to delaminate have high levels of apical CRB2. The basally-positioned nuclei of these apically constricted cells had low but detectable levels of SNAIL1 (Fig 5F-G'), suggesting that SNAIL1 accumulation begins at the time of apical constriction.

CRB2 and Myosin IIB on opposing cell edges

In *Drosophila*, cell edges enriched with Crumbs can direct Myosin II cable formation at other cell edges[20], and Myosin II (non-muscle myosin heavy chain II-B) has an important role in amniote gastrulation[24]. When viewed *en face*, Myosin IIB was present on most apical edges of wild-type E8.0 epiblast cells, but the intensity of expression was variable. In double labeling experiments, the levels of Myosin IIB and CRB2 on cell edges were inversely correlated: cell edges with high levels of CRB2 had lower levels of Myosin IIB, whereas cell edges with thicker myosin cables tended to have low levels of CRB2 (Fig. 6A-C). The reciprocal enrichment of CRB2 and Myosin IIB was also apparent in E7.0 early bud streak regions (Supplementary Fig. 6C) and in the epiblast adjacent to the streak at E8.5 (Supplementary Fig. 6D). The overall level of apical Myosin IIB assayed by immunofluorescence was ~2-fold lower in the mutants than in wild-type embryos (Fig. 6D, E), indicating that CRB2 promotes the apical enrichment of Myosin IIB.

The abnormal EMT disrupts the epiblast basement membrane

In older (E8.5) *Crumbs2* and *Poglut1*^{wsnp} mutants, we observed that the epiblast epithelium outside of the streak was ~1.4-fold thicker than in wild-type embryos (Fig. 7A, E). Individual cells of the anterior *Crumbs2* epiblast (the future neural epithelium) were taller and had smaller apical surfaces than those in wild type (Fig. 7B, D). This was not due to altered proliferation rates, as the frequency of mitotic cells was the same in the wild type and mutants (Supplementary Fig.7A); nor was it due to a breakdown in apical-basal polarity, as apical markers were localized correctly in the mutants (Supplementary Fig. 7B). Breaks in the basement membrane were detected in the mutant neural epithelium (Fig. 7A) and occasional cells expressing SOX2 were detected below the breaks in the basement membrane (Fig. 7A), demonstrating that integrity of the epiblast was compromised in the mutants at this stage.

To test whether CRB2 was required for integrity of the epiblast in older embryos because of events triggered by gastrulation, we blocked primitive streak formation genetically. *Wnt3* is required for the initiation of the primitive streak, but the *Wnt3* mutant epiblast continues to proliferate as an epithelium[25]. *Crumbs2 Wnt3* double mutants were indistinguishable in morphology from *Wnt3* single mutants (Fig. 7F). Sections stained for SOX2 and Laminin expression showed that the double mutant epiblast resembled that of the *Wnt3* single mutants (Fig. 7G, H): the basement membrane below the epiblast appeared to be intact (Fig. 7H) and no SOX2-positive nuclei were located below the basement membrane in the double mutants (Fig. 7H). We infer that the defects in epithelial organization of the *Crumbs2* epiblast are secondary to the gastrulation phenotype, which suggests that that the physical disruption caused by the absence of CRB2 at the primitive streak propagates through the contiguous epiblast epithelium.

DISCUSSION

The data presented here define a specific role for the apical protein CRB2 in promoting cell ingression during the epithelial-to-mesenchymal transition that generates the germ layers during mouse gastrulation. A previous analysis of the mouse *Crumbs2* mutant phenotype identified a defect in gastrulation[14]; that group inferred, based on the function of *Drosophila* Crumbs, that the gastrulation defect was secondary to disruption of apical-basal polarity in the epiblast. In contrast, we find that mouse embryos that lack all Crumbs proteins form an epiblast epithelium that expresses classical markers of apical-basal polarity in the correct pattern. The phenotype of the *Crumbs2* null mutant is recapitulated by deleting the gene specifically in cells of the primitive streak using *T-Cre*, demonstrating that CRB2 is specifically required in the cells of the primitive streak to promote the EMT.

Crumbs2 mutants show a striking block in cell ingression beginning at E7.5. The first steps of the EMT are successful in *Crumbs2* mutants: the basement membrane breaks down, and cells at the streak undergo apical constriction accompanied by a basal shift of the cell body. However, in the absence of CRB2, apical junctions do not dissolve, even as the cell body moves further away from the apical surface, leaving a long thin E-cadherin+ cytoplasmic connection to the apical surface of the epiblast.

The cells that accumulate at the streak in *Crumbs2* mutants express SOX2 rather than SNAIL1, suggesting that the expression of SNAIL1 depends on completion of the CRB2-dependent step

in cell ingression. As SNAIL1 represses expression of both SOX2 and E-cadherin during the EMT [9,26,27], the absence of SNAIL1 could also account for the failure to down-regulate E-cadherin in *Crumbs2* mutants. However, mouse embryos that lack SNAIL1 protein do make a mesoderm layer[27], indicating the failure to upregulate SNAIL1 is not sufficient to block cell ingression. We therefore infer that CRB2 has an additional role during the EMT.

CRB2 is localized in a striking anisotropic pattern in the apical epiblast. The accumulation of unequal levels of CRB2 on different cell edges is reminiscent of the distribution of planar cell polarity proteins, but there is no obvious polarity of the CRB2 distribution, suggesting that it is not dictated by a global clue. In chimeric embryos, wild-type epiblast cells adjacent to mutant cells lacked detectable CRB2 protein on the interface with the mutant cell (Fig. 4F and Supplementary Fig 4C), suggesting that stability of CRB2 depends on the formation of homophilic complexes with CRB2 on adjacent cells, as in *Drosophila* and zebrafish[20,21,22]. These data suggest that the complex CRB2 distribution in the apical epiblast is self-organizing: once a cell expresses high CRB2 on a cell edge adjacent to a CRB2-expressing cell, a positive feedback loop leads to accumulation of more CRB2 at that edge.

Although Myosin IIB is present at all cell edges of the mouse epiblast, the level of Myosin IIB is inversely correlated with the amount of CRB2 on that edge. In the invaginating *Drosophila* salivary gland placode, homophilic interactions between Crumbs proteins on adjacent cell edges recruit aPKC[20,28]. aPKC can phosphorylate and inactivate Rho-kinase, and Rho-kinase can activate myosin assembly[29]. Thus we hypothesize that aPKC is sequestered to cell edges with high CRB2, promoting myosin assembly on cell edges with low CRB2. Myosin cables under tension will recruit more myosin in a Rho-kinase dependent process[30]; such a positive feedback loop could reinforce the anisotropy of the myosin distribution in the mouse epiblast (Fig. 6F).

We suggest that the unequal distribution of CRB2 protein is an essential component of a local mechanism that determines which cells will ingress from the epithelium. As high levels of CRB2 correlate with lower levels of Myosin IIB, the final stage of cell ingression during the EMT may occur by basal cell extrusion, where myosin contraction in cells neighboring a high CRB2-expressing cell pushes the adjacent CRB2+ cell out of the epithelium. This process may resemble apical cell extrusion, which removes dying cells from epithelia[31] and the basal cell extrusion that takes place during metastasis[32]. Generation of new transgenic reporters for live

imaging of the dynamics of Myosin IIB and CRB2 should help define the events and mechanisms of cell ingression during this EMT.

Our findings fit with a recent model that ingression of cells at the primitive streak is a population event controlled by dynamic, self-reinforcing cell interactions[4], and place the CRB2 protein complex at a central node in these interactions. In this view, CRB2 anisotropy helps determine which cells will ingress at the streak while promoting the mechanical process of ingression. In addition, forces generated at the streak in the absence of CRB2 affect the integrity of the contiguous epithelium of the epiblast, consistent with a role for Crumbs proteins in global tissue integrity during dynamic tissue rearrangements[11,33].

Heritable mutations in *CRB2* have been identified in childhood-onset kidney disease [34,35], and abnormal epithelial-to-mesenchymal transitions are associated with renal fibrosis[36,37]. EMTs have been implicated in tumor progression, and both amplification and point mutations in *CRB2* have been identified in large-scale cancer genome sequencing projects[38,39,40,41]. Cell biological studies to test the functional significance of these *CRB2* mutations should provide new perspectives on tissue dynamics in human disease and cancer progression.

Author Contributions

NR carried out the experiments, TO participated in and analyzed the live imaging experiments. NFS-G, CJM and JW provided essential reagents and advice. NR and KVA designed experiments, analyzed the data and wrote the paper.

Acknowledgements

We thank the MSKCC Molecular Cytology and Mouse Genetics Core Facilities for valuable technical support. We thank the Hadjantonakis lab for the X-linked GFP and GFP-GPI strains. We thank Mark Lewandoski for *Brachyury-Cre* mice. We thank Jennifer Zallen, Anna-Katerina Hadjantonakis, Alan Hall, Isabelle Migeotte, Hemant Kakkar and members of the Anderson lab for their helpful suggestions. The work was supported by NIH R37 HD03455 to KVA and the MSKCC Cancer Center Support Grant (P30 CA008748).

Figure Legends

Figure 1: *Crumbs2* is required for mammalian gastrulation

(A) In situ hybridization for *Meox1* expression in wild type, *Crumbs2* mutant, *Crumbs2 Crumbs3* and *Crumbs1*^{rd8} *Crumbs2* double mutants at E8.5. The double mutants have the same reduction in paraxial mesoderm seen in *Crumbs2* mutants, n ≥ 4 embryos for each genotype. (B) Wild type, *Crumbs2* mutants and *Crumbs* triple mutants (*Crumbs1*^{rd8}, *Crumbs2*$^{-/-}$, *Crumbs3*$^{-/-}$) at E7.5 probed for expression of *Brachyury*, a marker of the primitive streak, n ≥ 3 embryos for each genotype. The extraembryonic portion of the triple mutant was removed for genotyping (C) Transverse sections through the epiblast of E7.75 wild type and *Crumbs2*$^{-/-}$ *Crumbs3*$^{-/-}$ double mutant embryos immunostained for ZO1 and pERM, aPKCλ and Par3 and γ-tubulin and ARL13b, n=3 double mutant embryos (3-4 sections per embryo). The double mutants do not have defects in apical-basal polarity of the epiblast. Single optical sections of transverse sections through the primitive streak at E7.5 (D, E) and E8.0 (F) of WT (D, E), *Crumbs2* (D, E, F) and *Poglut1*^{wsnp} (F) immunostained for Brachyury (T) and Laminin (D), SNAIL1 and SOX2 (E, F), n ≥ 5 mutant embryos per genotype. Posterior to the right; bars indicate width of primitive streak. At E7.5, a few cells expressing SOX2 accumulate at the streak (line in E). At this stage, the SNAIL1+ mesoderm layer is 2-3 cells thick in wild type, and 1-2 cells thick in the mutant. By E8.0, many SOX2+ cells, and scattered SNAIL1+ cells, have accumulated in the *Crumbs2* and *Poglut1*^{wsnp} primitive streak region (F). (A) Dorsal view, anterior up, (B) Lateral view, anterior to left, distal down. (C) Apical is up. Scale bars in A and B, 50μm; C-F, 21μm. The images shown here are representative and are of the mutant and wild type from the same experiment.

Figure 2: *Crumbs2* promotes cell ingression at the primitive streak

(A-C) Scanning electron microscope views of the primitive streak in fractured wild-type (A, A'), *Crumbs2* (B, B') and *Poglut1*^{wsnp} (C,C') embryos at E7.75, n ≥ 6 embryos per genotype; posterior to the right. A', B' and C' are higher magnification of the boxed regions in A, B and C respectively. Arrows point to long constricted apical segments of primitive streak cells in the mutants. (D-F) Single optical section from 3-D reconstruction of transverse sections through the primitive streak immunostained for E-cadherin (red) of wild type (D), *Crumbs2* (E) and *Poglut1*^{wsnp} (F) embryos expressing X-linked GFP in a mosaic manner, n ≥ 5 X-GFP positive embryos per genotype. Arrows show thin E-cadherin-positive cytoplasmic connections to the apical surface of cells, with the cell base (nuclei) far from the epiblast surface. (G-H) 3-D reconstructions of individual GFP-expressing single cells from the primitive streak of wild-type

(G) and *Crumbs2* mutants (H) carrying the X-GFP transgene, showing the elongated cytoplasmic threads that connect ingressing mutant cells to the apical surface of the epiblast (apical to the left), n ≥ 5 X-GFP positive embryos per genotype. Scale bar (A-C' and G-H),10 μm; D-F, 25 μm. The images shown here represent the mutant and wild type from the same experiment.

Figure 3: Live imaging defines defects in cell ingression in *Crumbs2* mutants

Individual cells delaminating at the primitive streak (highlighted yellow) in snapshots from time-lapse imaging of wild-type (A) and *Crumbs2* (B) mutant embryos with mosaically labeled cells using the mT/mG system. Apical is up in these transverse optical sections. In wild-type embryos (A), the cell constricts its apical membrane and detaches its apical connection to delaminate from the epithelium in less than 2 hours (arrows showing loss of apical connection/retraction tail). In *Crumbs2* mutants (B), the cell constricts its apical membrane and sends out basal protrusions but fails to leave the epithelium. Time interval: 10 minutes. Apical side of the epithelium is up. (C) Quantitative analysis of cell shape at the streak in wild-type and *Crumbs2* mutant embryos. Membrane GFP-expressing cells were depicted manually for cell surface rendering and ellipticity was plotted for wild-type and *Crumbs2* mutant streak cells to compare cell shape. Wild-type cells at the streak were predominantly oblate ellipsoids (flattened spheroids); long axes parallel to the epiblast surface (e = 0.34 ± 0.01 (mean ± SEM), n=102 structures from 9 cells, 4 independent experiments), whereas mutant cells were prolate ellipsoids (cigar-shaped) with long axes perpendicular to the epiblast surface (e = 0.17 ± 0.01 (mean ± SEM), n=169 structures from 13 cells, 3 independent experiments) (unpaired t-test: $p < 0.0001$). (D) Ingression dynamics of streak cells. The apical surface area was determined from optical confocal sections of GFP-labeled cells from time-lapse images at the apical surface of streak cells. The apical surface of wild-type cells reduced over time, whereas the mutant cells stuck at the streak have a constant small apical surface area. Pink bar marks the onset of ingression in wild type. Scale bars A, B,10 μm.

Figure 4: Streak-autonomous and non-cell autonomous activities of *Crumbs2*

(A) *Meox1* expression at E8.5 shows the reduction in paraxial mesoderm in embryos with conditional deletion of *Crumbs2* in cells of the primitive streak using *T-Cre*, compared to WT, n = 3 embryos per genotype. (B) Single optical section of transverse sections through the primitive streak region of WT and *T-CRE, Crumbs2^{flox}/Crumbs2^{-}* embryos at E8.5 immunostained for SNAIL1 and SOX2, n = 3 embryos per genotype (2-3 sections per embryo).

Conditional deletion of *Crumbs2* with *T-Cre* leads to accumulation of SOX2+ cells at the primitive streak similar to *Crumbs2* null mutants. (C) Schematic showing the generation of mouse chimeras with *Crumbs2*$^{-/-}$ mutant cells labeled with GPI-GFP. (D-E) Contribution of *Crumbs2*$^{-/-}$ cells to normal tissues in chimeras. Transverse cryosection (D) and single optical section of whole mount immunostaining (E) through chimeric embryos with moderate contribution of *Crumbs2* mutant cells (green) stained with phalloidin (red) showing the contribution of mutant cells to neural epithelium and otic vesicle (D) and somites (E) (F) *En face* view of the streak epithelium of chimeric embryos at E8.5 immunostained for Crumbs2 (red) and phalloidin (white-F'''). Mutant cells are GFP positive. Arrows point to the absence of CRB2 expression in wild-type cells at the edges shared with mutant cells, whereas phalloidin expression was maintained at these edges. Asterisk highlights an exceptional cell at the streak that retains CRB2 despite being adjacent to *Crumbs2* mutant cells. Scale bars A, 150 μm; B, D, E, 40 μm; F,10 μm. The images shown here are representative and show the mutant and wild type from the same experiment. (D-F) n=10 chimeric embryos were analyzed by cross section for contribution to different tissues and n=10 chimeric embryos were used for immunostaining and enface visualization of proteins (n=5 chimeric embryos for Crb2, Phalloidin and n=5 chimeric embryos for Crb2, ß-catenin).

Figure 5: CRB2 enrichment at the primitive streak

(A, B) Double staining of CRB2 and phalloidin at early primitive streak stages, posterior to the right. (A, A') At E6.75, CRB2 is enriched in the posterior epiblast, including the region of the primitive streak. Posterior epiblast from A is magnified in A'. (B, B'). At E7.75 CRB2 is expressed in both the anterior presumptive neural epithelium and the epiblast and is enriched in the posterior epiblast. (B') Higher magnification of streak region. (C, C') *En face* view of the apical surface of E8.5 posterior epiblast cells; proximal is up. Extended projection view of the same region of the primitive streak stained for ZO1(C) and CRB2 (D). ZO1 is expressed at uniform levels on all cell edges, whereas the level of expression of CRB2 is highly variable between cells and at different edges of the same cell. Neither *Crumbs2* RNA nor CRB2 protein was detected in the wild-type endoderm or mesoderm (Fig. 5A, A'; Supplementary Fig. 1). (E, E') 3D reconstruction from whole mount immunostaining for CRB2 in wild-type E8.0 embryos that express the X-linked GFP transgene, highlight the shape of individual cells. Apically constricted cells have high levels of apical CRB2. (F-G') 3D reconstruction from whole mount immunostaining for SNAIL1 in wild type X-GFP embryos at E8.0. SNAIL1 is detectable in the basal nuclei of apically constricted cells in the epiblast layer of the wild-type streak. Black bar

indicates the position of the streak. Cells of the wild-type mesoderm layer (bottom) are strongly Snail1+ (red), whereas some apically constricted GFP+ cells of the epiblast layer (top) have detectable levels of Snail1 in their basally-positioned nuclei (rightward arrows). Note the thin GFP+ cytoplasmic connection to the apical surface of the Snail+ cell in (F) (leftward arrow). Scale bars A, B, 100 μm; C-G', 10 μm. Each immunostaining experiment contained at least 5-6 wild type embryos with and without X-GFP each. The images shown here are representative. This staining was repeated a minimum of three independent times to ensure reproducibility.

Figure 6: CRB2 regulates the distribution of Myosin IIB

(A) *En face* view of the apical surface of the epiblast layer of the primitive streak at E8.0, showing the reciprocal enrichment of CRB2 and Myosin IIB on different cell edges; proximal is up. (A) Single optical section of whole mount immunostaining for CRB2 (red) and Myosin IIB (green). (B) Magnification of boxed region in A, with single channels for CRB2 and Myosin. (C) Quantification of Myosin IIB and CRB2 en face localization at cell edges at the primitive streak (see Methods). Cell edges with high CRB have low levels of Myosin IIB (normalized intensity of Myosin IIB at high Myosin edges = 1.48 (n=349 cell edges) and normalized intensity of Myosin IIB at high CRB2 edges = 0.6 (n=436 cell edges); two tailed student t-test, $p<0.00001$, n=5 wild-type embryos). Edges with high Myosin IIB have low levels of CRB2 (normalized intensity of CRB2 at high Myosin edges = 0.57 (n=349 cell edges) and normalized intensity of CRB2 at high CRB2 edges = 1.36 (n=436 cell edges); two tailed student t-test, $p <0.00001$. The box represents the 25^{th} -75^{th} percentile, whiskers indicate 1.5 times the range, dots are the outliers and bar in the middle is median. (D-E) Myosin IIB along the cell edges is reduced in *Crumbs2* mutants. (D) Extended projection view of the primitive streak of embryos whole mount stained for Myosin IIB and phalloidin at E8.0 showing lower levels on Myosin IIB on the cell edges in *Crumbs2* compared to wild-type embryos. (E) Quantification of relative staining intensity shows that the total level of Myosin IIB on cell edges is ~2 fold higher in wild type than in *Crb2* mutants (WT mean myosin intensity: 17.25 $x10^3$, n=570 edges, 4 wild-type embryos; mutant mean myosin intensity: 9.32 $x10^3$; n= 570 edges, 3 mutant embryos, two tailed student t-test, $p <0.00001$). The box represents the 25^{th} -75^{th} percentile, whiskers indicate 1.5 times the range, dots are the outliers and bar in the middle is median. Scale bars A and B, 10 μm; D, 20 μm. (F) Model for actions of CRB2. CRB2 controls E-cadherin down-regulation by promoting the SOX2-to-SNAIL1 switch, and controls Myosin IIB accumulation through a second pathway, perhaps through aPKC and Rho kinase. The complex anisotropic patterns of CRB2 and Myosin IIB are

regulated in part by self-organizing regulatory mechanisms. The images shown represent the mutant and wild type from the same experiment.

Figure 7: CRB2 is required for epiblast integrity at the primitive streak only when cells delaminate at the streak

(A) Single optical sections of transverse section through the anterior epiblast/presumptive neural epithelium of wild-type and *Crumbs2* mutants immunostained for SOX2 and Laminin show the increased thickness of the neural epithelium in the mutants at E8.0. (B) *En face* views of the surface of the anterior epiblast of wild type and *Crumbs2* stained with ZO1 show the reduction in the apical surface area of the cells in the *Crumbs2* mutants. (C) 3D reconstruction of cells in the neural epithelium of wild type and *Crumbs2*$^{-/-}$ embryos expressing X-linked GFP and stained for ZO1. The cells in the mutants have reduced apical surface area and an increased basolateral domain; ZO1 is expressed in the correct apical domain. (D) Quantification of apical cell surface area of cells in the wild-type and *Crumbs2* mutant anterior epiblast/presumptive neural epithelium (mean ± SEM), WT = 23.64±0.60, n=559 cells, 4 embryos and *Crumbs2*$^{-/-}$ = 10.50±0.34, n=471 cells, 5 embryos, $p<0.0001$. (E) Quantification of neural epithelial thickness (mean ± SEM), WT = 37.75±0.92, n=15 anterior epiblast and *Crumbs2*$^{-/-}$=53.25±1.60, n=14 anterior epiblast, $p<0.0001$. (F) *Wnt3*$^{-/-}$ and *Crumbs2*$^{-/-}$ *Wnt3*$^{-/-}$ double mutant embryos are morphologically identical. *Wnt3*$^{-/-}$ mutants do not form a primitive streak and develop as a bag of epithelial cells (n=8 double mutant embryos). (G) Transverse section through the embryos immunostained for Laminin (green) and SOX2 (red), n=5 double mutant embryos. (H) Higher magnification of the epithelium of *Wnt3*$^{-/-}$ and *Wnt3*$^{-/-}$ *Crumbs2*$^{-/-}$embryos shows that the double mutants do not have breaks in laminin expression or SOX2 positive nuclei below the basement membrane. Scale bars A-C, G-H, 21 μm; F,150 μm. The images shown here are representative and show the mutant and wild type from the same experiment.

References

1. Shook, D. & Keller, R. Mechanisms, mechanics and function of epithelial-mesenchymal transitions in early development. *Mech. Dev*. **120,** 1351-1383 (2003).

2. Nieto, M. A., Huang, R.Y., Jackson, R. A; & Thiery, J. P. EMT: 2016*. Cell* **166**: 21-45. (2016).

3. Williams, M., Burdsal, C., Periasamy, A., Lewandoski, M. & Sutherland, A. Mouse primitive streak forms in situ by initiation of epithelial to mesenchymal transition without migration of a cell population. *Dev. Dyn*. **241,** 270-283 (2012).

4. Voiculescu, O., Bodenstein, L., Lau, I. J. & Stern, C. D. Local cell interactions and self-amplifying individual cell ingression drive amniote gastrulation. *eLife*. **3,** e01817 (2014).

5. Herion, N. J., Salbaum, J. M. & Kappen, C. Traffic jam in the primitive streak: the role of defective mesoderm migration in birth defects. *Birth Defects Res. A Clin. Mol. Teratol*. **100,** 608-622 (2014).

6. Thiery, J. P., Acloque, H., Huang, R. Y. & Nieto, M. A. Epithelial-mesenchymal transitions in development and disease. *Cell.* **139,** 871-890 (2009).

7. Scheel, C. & Weinberg, R. A. Cancer stem cells and epithelial-mesenchymal transition: concepts and molecular links. *Semin. Cancer Biol*. **22,** 396-403 (2012).

8. Arnold, S. J. & Robertson, E. J. Making a commitment: cell lineage allocation and axis patterning in the early mouse embryo. *Nat. Rev. Mol. Cell Biol*. **10,** 91-103 (2009).

9. Acloque, H., *et al.* Reciprocal repression between Sox3 and snail transcription factors defines embryonic territories at gastrulation. *Dev. Cell.* **21,** 546-558 (2011).

10. Tepass, U., Theres, C. & Knust, E. Crumbs encodes an EGF-like protein expressed on apical membranes of *Drosophila* epithelial cells and required for organization of epithelia. *Cell*. **61,** 787-799 (1990).

11. Tepass, U. Crumbs, a component of the apical membrane, is required for zonula adherens formation in primary epithelia of *Drosophila*. *Dev. Biol.* **177,** 217-225 (1996).

12. van de Pavert, S. A. *et al.* Crumbs homologue 1 is required for maintenance of photoreceptor cell polarization and adhesion during light exposure. *J. Cell. Sci.* **117,** 4169-4177 (2004).

13. Whiteman, E. L. *et al.* Crumbs3 is essential for proper epithelial development and viability. *Mol. Cell. Biol.* **34,** 43-56 (2014).

14. Xiao, Z. *et al.* Deficiency in Crumbs homolog 2 (Crb2) affects gastrulation and results in embryonic lethality in mice. *Dev. Dyn.* **240,** 2646-2656 (2011).

15. Ramkumar, N. *et al.* Protein O-Glucosyltransferase 1 (POGLUT1) promotes mouse gastrulation through modification of the apical polarity protein CRUMBS2. *PLoS Genet.* **11,** e1005551 (2015).

16. Hadjantonakis, A. K., Cox, L. L., Tam, P. P. & Nagy, A. An X-linked GFP transgene reveals unexpected paternal X-chromosome activity in trophoblastic giant cells of the mouse placenta. *Genesis* **29,** 133-140 (2001).

17. Hayashi, S., Lewis, P., Pevny, L. & McMahon, A. P. Efficient gene modulation in mouse epiblast using a Sox2Cre transgenic mouse strain. *Mech. Dev.* **119 Suppl 1,** S97-S101 (2002).

18. Perantoni, A. O. *et al.* Inactivation of FGF8 in early mesoderm reveals an essential role in kidney development. *Development* **132,** 3859-3871 (2005).

19. Rhee, J. M. *et al. In vivo* imaging and differential localization of lipid-modified GFP-variant fusions in embryonic stem cells and mice. *Genesis* **44,** 202-218 (2006).

20. Röper, K. Anisotropy of Crumbs and aPKC drives myosin cable assembly during tube formation. *Dev. Cell.* **23,** 939-953 (2012).

570 21. Letizia, A., Ricardo, S., Moussian, B., Martín, N. & Llimargasm, M. A functional role of the
571 extracellular domain of Crumbs in cell architecture and apicobasal polarity. *J. Cell. Sci.* **126,**
572 2157-2163 (2013).
573
574 22. Zou, J., Wang, X. & Wei, X. Crb apical polarity proteins maintain zebrafish retinal cone
575 mosaics via intercellular binding of their extracellular domains. *Dev. Cell*. **22,** 1261-1274 (2012).
576
577 23. Tepass, U. The apical polarity protein network in *Drosophila* epithelial cells: regulation of
578 polarity, junctions, morphogenesis, cell growth, and survival. *Annu. Rev. Cell Dev. Biol.* **28,** 655-
579 685 (2012).
580
581 24. Rozbicki, E. *et al.* Myosin-II-mediated cell shape changes and cell intercalation contribute to
582 primitive streak formation. *Nat. Cell Biol.* **17,** 397-408 (2015).
583
584 25. Liu, P. *et al.* Requirement for Wnt3 in vertebrate axis formation. *Nat. Genet.* **22,** 361-365
585 (1999).
586
587 26. Ciruna, B. & Rossant, J. FGF signaling regulates mesoderm cell fate specification and
588 morphogenetic movement at the primitive streak. *Dev. Cell.* **1,** 37-49 (2001).
589
590 27. Carver, E. A., Jiang, R., Lan, Y., Oram, K.F. & Gridley, T. The mouse snail gene encodes a
591 key regulator of the epithelial-mesenchymal transition. *Mol. Cell. Biol*. **21,** 8184-8188 (2001).
592
593 28. Fletcher, G. C., Lucas, E. P., Brain, R., Tournier, A. & Thompson, B. J. Positive feedback
594 and mutual antagonism combine to polarize Crumbs in the *Drosophila* follicle cell epithelium.
595 *Curr. Biol.* **22,** 1116-1122 (2012).
596
597 29. Ishiuchi, T., & Takeichi, M. Willin and Par3 cooperatively regulate epithelial apical
598 constriction through aPKC-mediated ROCK phosphorylation. *Nat Cell Biol.* **13,** 860-866 (2011).
599
600 30. Fernandez-Gonzalez, R., Simoes Sde, M., Röper, J. C., Eaton, S. & Zallen, J. A. Myosin II
601 dynamics are regulated by tension in intercalating cells. *Dev. Cell.* **17,** 736-743 (2009).
602

603 31. Slattum, G., McGee, K. M. & Rosenblatt, J. P115 RhoGEF and microtubules decide the
604 direction apoptotic cells extrude from an epithelium. *J. Cell. Biol.* **186,** 693-702 (2009).
605
606 32. Slattum, G. M. & Rosenblatt, J. Tumour cell invasion: an emerging role for basal epithelial
607 cell extrusion. *Nat. Rev. Cancer*. **14,** 495-501 (2014).
608
609 33. Campbell, K., Knust, E. & Skaer H. Crumbs stabilises epithelial polarity during tissue
610 remodelling. *J. Cell Sci.* **122,** 2604-2612 (2009).
611
612 34. Ebarasi, L. *et al.* Defects of CRB2 cause steroid-resistant nephrotic syndrome. *Am. J. Hum.*
613 *Genet*. **96,** 153-161 (2015).
614
615 35. Slavotinek, A. *et al.* CRB2 mutations produce a phenotype resembling congenital nephrosis,
616 Finnish type, with cerebral ventriculomegaly and raised alpha-fetoprotein. *Am. J. Hum. Genet*.
617 **96,** 162-169 (2015).
618
619 36. Grande, M.T. *et al.* Snail1-induced partial epithelial-to-mesenchymal transition drives renal
620 fibrosis in mice and can be targeted to reverse established disease. *Nat. Med.* **21,** 989-997
621 (2015).
622
623 37. Lovisa, S. *et al.* Epithelial-to-mesenchymal transition induces cell cycle arrest and
624 parenchymal damage in renal fibrosis. *Nat. Med.* **21,** 998-1009 (2015).
625
626 38. Arcila, M. E*. et al.* MAP2K1 (MEK1) Mutations Define a Distinct Subset of Lung
627 Adenocarcinoma Associated with Smoking. *Clin. Cancer Res*. **21,** 1935-1943 (2015).
628
629 39. Beltran, H. *et al*. Divergent clonal evolution of castration-resistant neuroendocrine prostate
630 cancer. *Nat. Med.* **22,** 298-305 (2016).
631
632 40. Cerami, E. *et al.* The cBio Cancer Genomics Portal: An Open Platform for Exploring
633 Multidimensional Cancer Genomics Data. *Cancer Discov.* **2,** 401-404 (2012).
634
635 41. Gao, J. *et al.* Integrative analysis of complex cancer genomics and clinical profiles using the
636 cBioPortal. *Sci. Signal*. **6,** p11 (2013).

637
638 42 Alves, C. H. *et al.* Loss of CRB2 in the mouse retina mimics human retinitis pigmentosa due
639 to mutations in the CRB1 gene. *Hum. Mol. Genet.* **22,** 35-50 (2013).
640
641 43. Barrow, J. R. *et al.* Ectodermal Wnt3/beta-catenin signaling is required for the establishment
642 and maintenance of the apical ectodermal ridge. *Genes Dev.* **17,** 394-409 (2003).
643
644 44. Mehalow, A. K. *et al.* CRB1 is essential for external limiting membrane integrity and
645 photoreceptor morphogenesis in the mammalian retina. *Hum. Mol. Genet.* **12,** 2179-2189
646 (2003).
647
648 45. Muzumdar, M. D., Tasic, B., Miyamichi, K., Li, L. & Luo, L. A global double-fluorescent Cre
649 reporter mouse. *Genesis* **45,** 593-605 (2007).
650
651 46. Lakso, M. *et al.* Efficient in vivo manipulation of mouse genomic sequences at the zygote
652 stage*. Proc. Natl. Acad. Sci. U.S.A.* **93,** 5860-5865 (1996).
653
654 47. Lee, J. D., Silva-Gagliardi, N. F., Tepass, U., McGlade, C. J. & Anderson, K. V. The FERM
655 protein Epb4.1l5 is required for organization of the neural plate and for the epithelial-
656 mesenchymal transition at the primitive streak of the mouse embryo. *Development* **134,** 2007-
657 2016 (2007).
658
659 48. Laprise, P. *et al.* The FERM protein Yurt is a negative regulatory component of the Crumbs
660 complex that controls epithelial polarity and apical membrane size. *Dev. Cell.* **11,** 363-374
661 (2006).
662
663 49. Franci, C. *et al.* Expression of Snail protein in tumor-stroma interface. *Oncogene* **25,** 5134-
664 5144 (2006).
665
666 50. Lemmers C, Médina E, Delgrossi MH, Michel D, Arsanto JP, Le Bivic A. hINADl/PATJ, a
667 homolog of discs lost, interacts with crumbs and localizes to tight junctions in human epithelial
668 cells. *J. Biol. Chem*. **277**, 25408-25415. (2002)
669

51. Caspary, T., Larkins, C.E., & Anderson, K.V. The graded response to Sonic Hedgehog depends on cilia architecture. *Dev. Cell.* **12,** 767-778 (2007).

52. Migeotte, I., Grego-Bessa, J. & Anderson, K. V. Rac1 mediates morphogenetic responses to intercellular signals in the gastrulating mouse embryo. *Development*. **138,** 3011-3020 (2011).

53. Silva, J. *et al.* Promotion of reprogramming to ground state pluripotency by signal inhibition. *PLoS Biol.* **6,** e253 (2008).

54. Li, Z., Wang, L., Hays, T.S., & Cai, Y. Dynein-mediated apical localization of crumbs transcripts is required for Crumbs activity in epithelial polarity. *J Cell Biol.* **180,** 31-38 (2008).

Figure 1

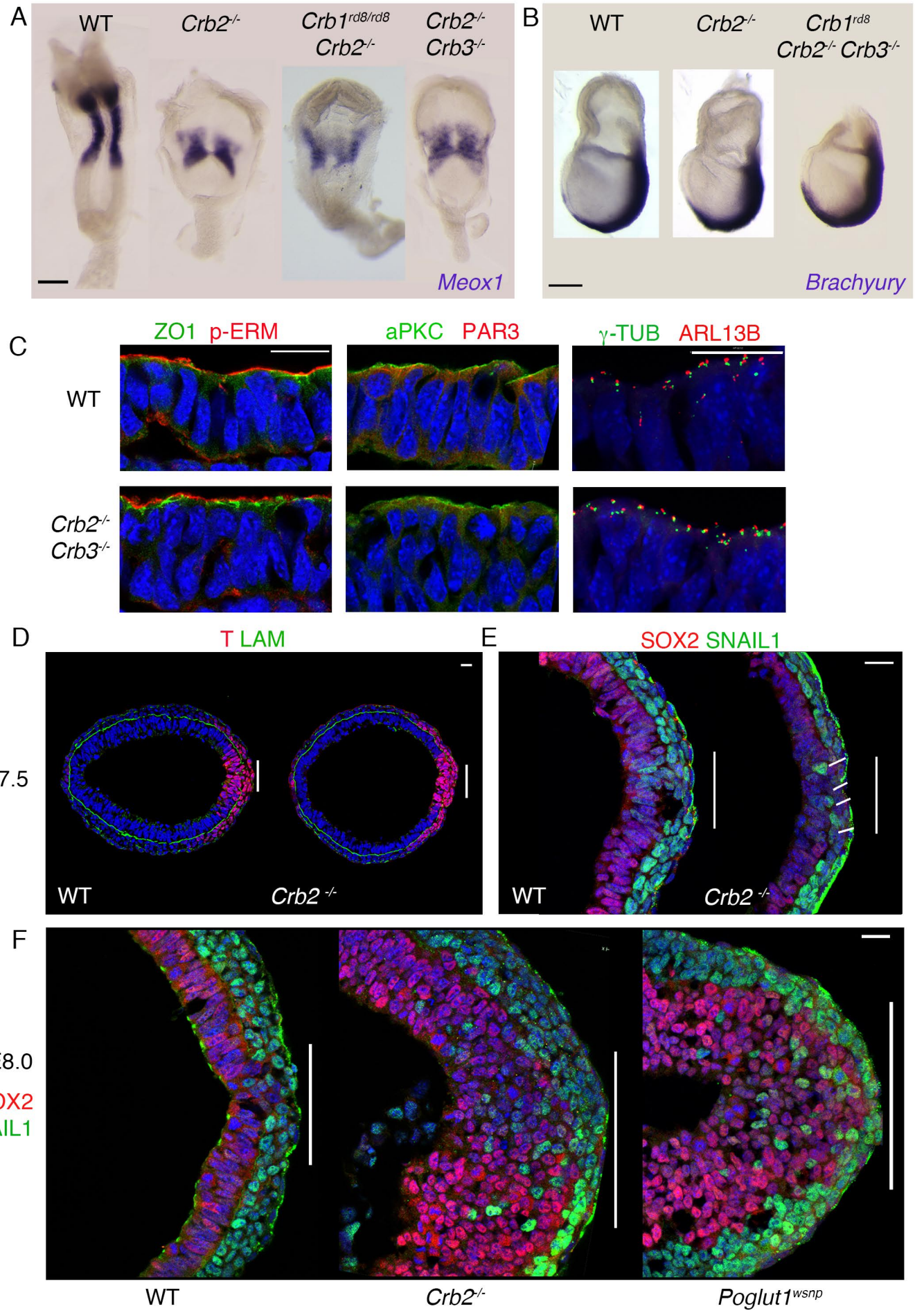
A
WT
Crb2-/-
Crb1rd8/rd8 Crb2-/-
Crb2-/- Crb3-/-
Meox1
B
WT
Crb2-/-
Crb1rd8 Crb2-/- Crb3-/-
Brachyury
C
ZO1 p-ERM
aPKC PAR3
γ-TUB ARL13B
WT
Crb2-/- Crb3-/-
D
T LAM
E7.5
WT
Crb2 -/-
E
SOX2 SNAIL1
WT
Crb2 -/-
F
E8.0
SOX2
SNAIL1
WT
Crb2-/-
Poglut1wsnp

Figure 2

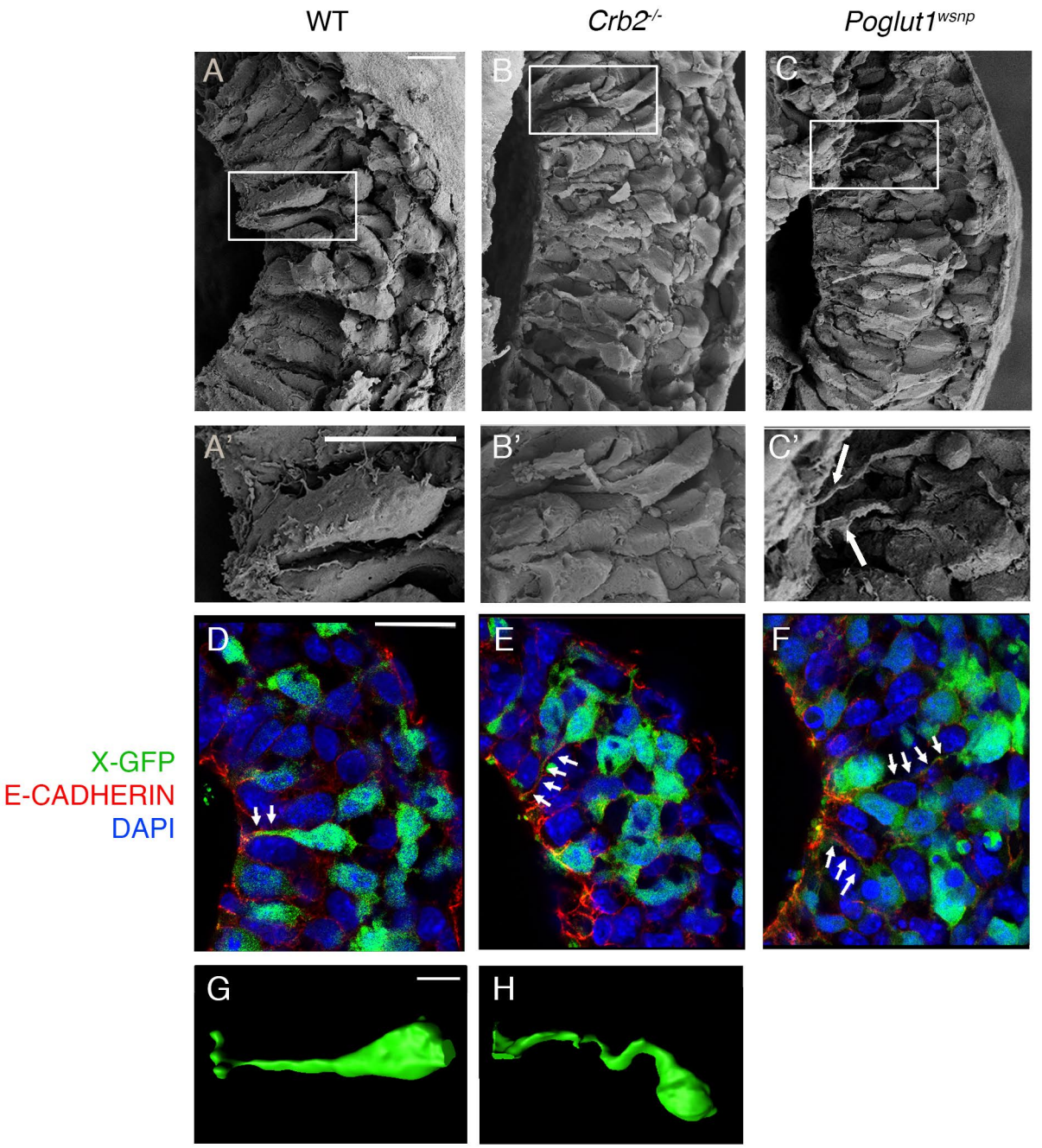

Figure 3

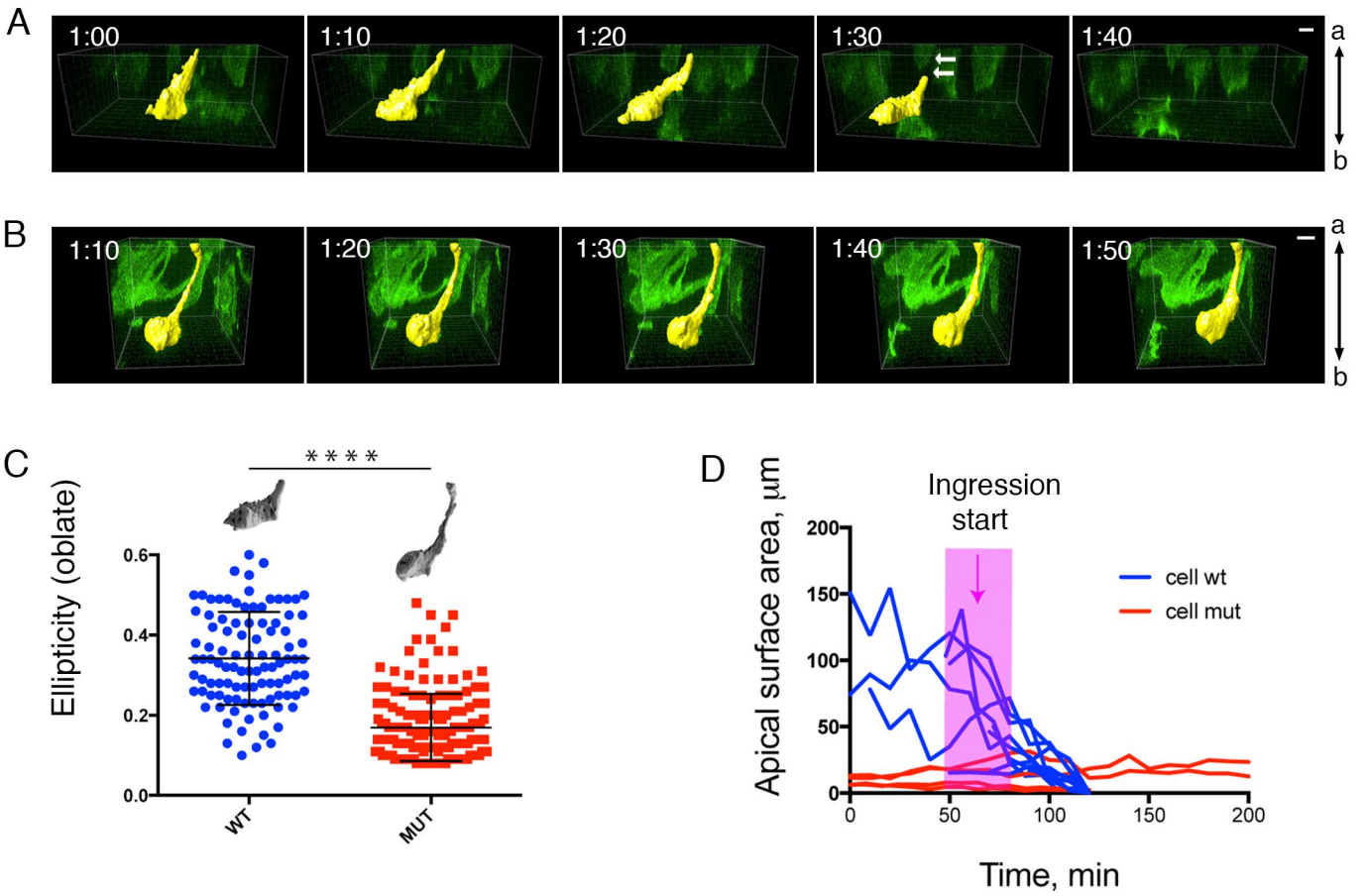
A
1:00
1:10
1:20
1:30
1:40
a
b
B
1:10
1:20
1:30
1:40
1:50
a
b
C
****
Ellipticity (oblate)
0.6
0.4
0.2
0.0
WT
MUT
D
Ingression start
Apical surface area, µm
200
150
100
50
0
0
50
100
150
200
Time, min
cell wt
cell mut

Figure 4

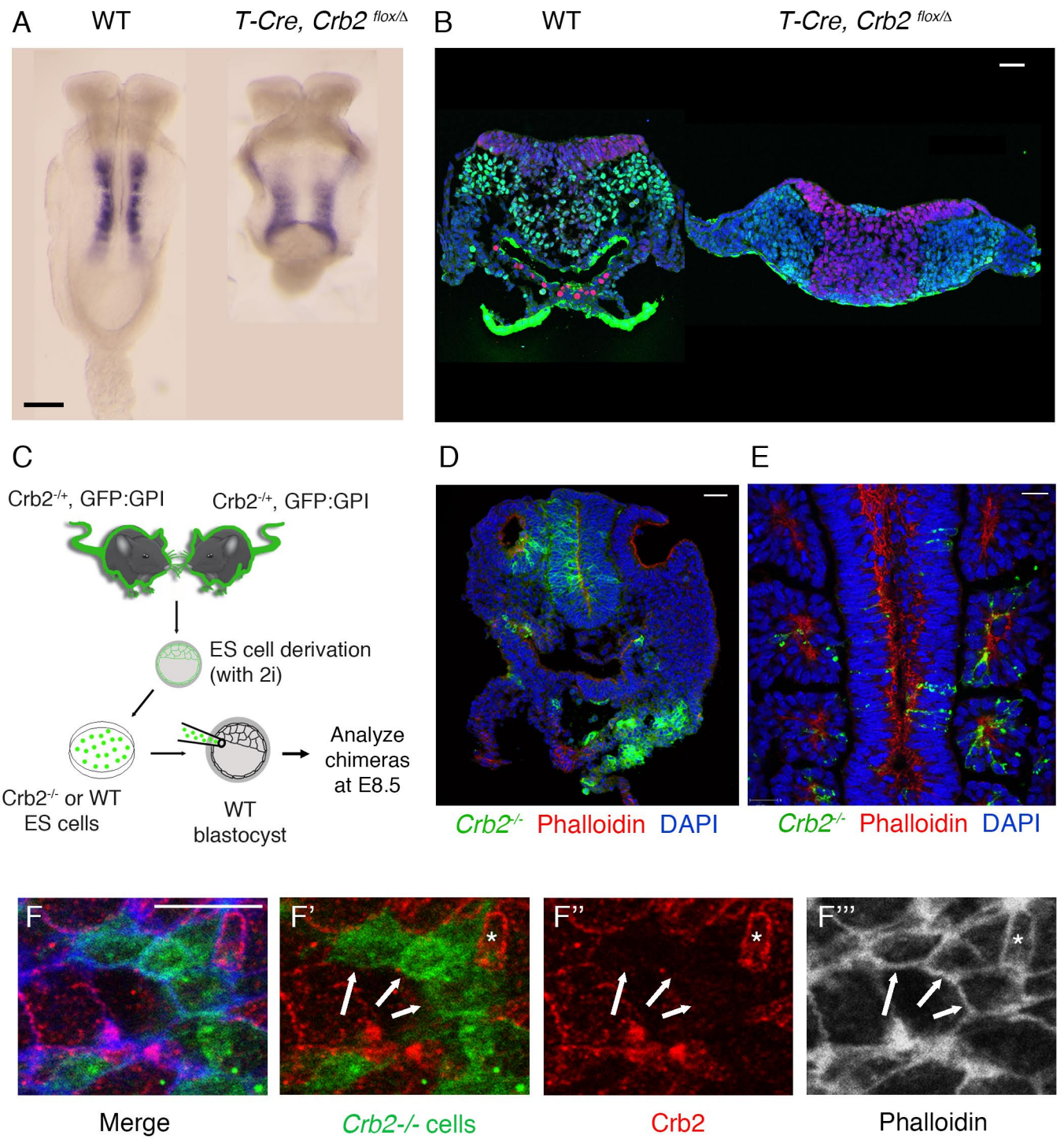
A
WT
T-Cre, Crb2 flox/Δ
B
WT
T-Cre, Crb2 flox/Δ
C
Crb2-/+, GFP:GPI
Crb2-/+, GFP:GPI
ES cell derivation
(with 2i)
Crb2-/- or WT
ES cells
WT
blastocyst
Analyze
chimeras
at E8.5
D
E
Crb2-/- Phalloidin DAPI
Crb2-/- Phalloidin DAPI
F
F'
F''
F'''
Merge
Crb2-/- cells
Crb2
Phalloidin

Figure 5

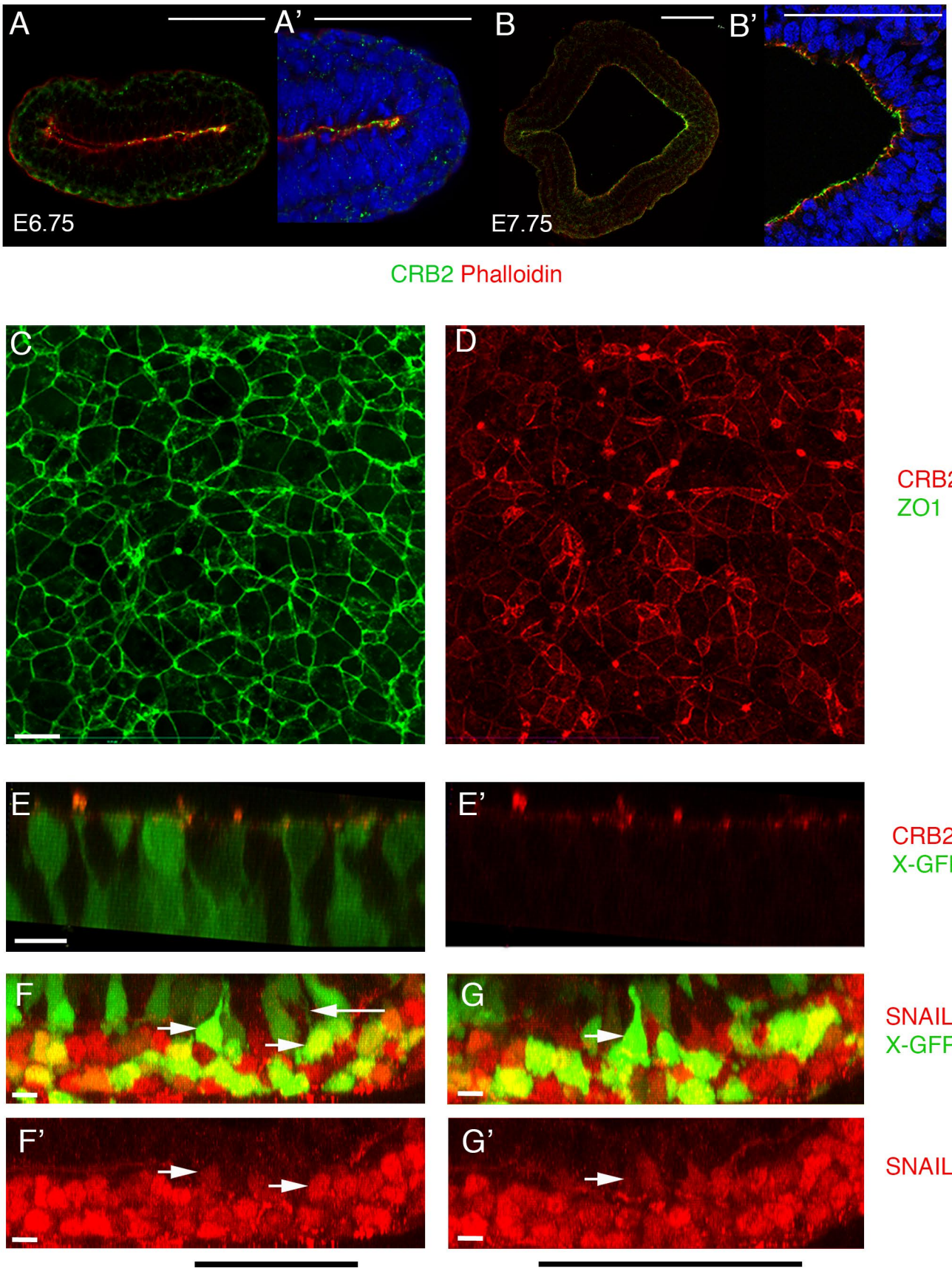
A
A'
B
B'
E6.75
E7.75
CRB2 Phalloidin
C
D
CRB2
ZO1
E
E'
CRB2
X-GFP
F
G
SNAIL1
X-GFP
F'
G'
SNAIL1

Figure 6

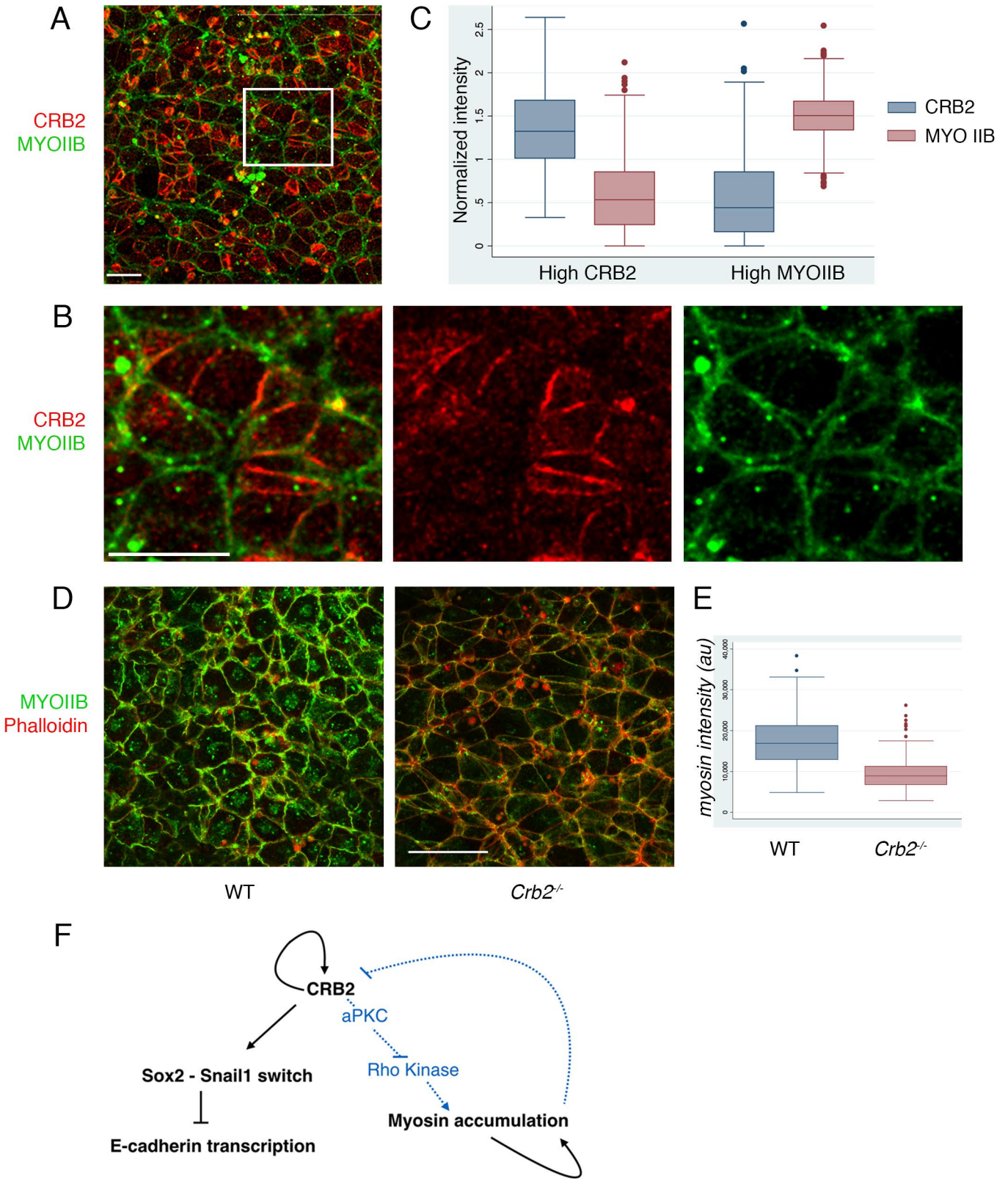
A
CRB2
MYOIIB
C
Normalized intensity
0
.5
1
1.5
2
2.5
High CRB2
High MYOIIB
CRB2
MYO IIB
B
CRB2
MYOIIB
D
MYOIIB
Phalloidin
WT
Crb2-/-
E
myosin intensity (au)
0
10,000
20,000
30,000
40,000
WT
Crb2-/-
F
CRB2
aPKC
Rho Kinase
Sox2 - Snail1 switch
E-cadherin transcription
Myosin accumulation

Figure 7

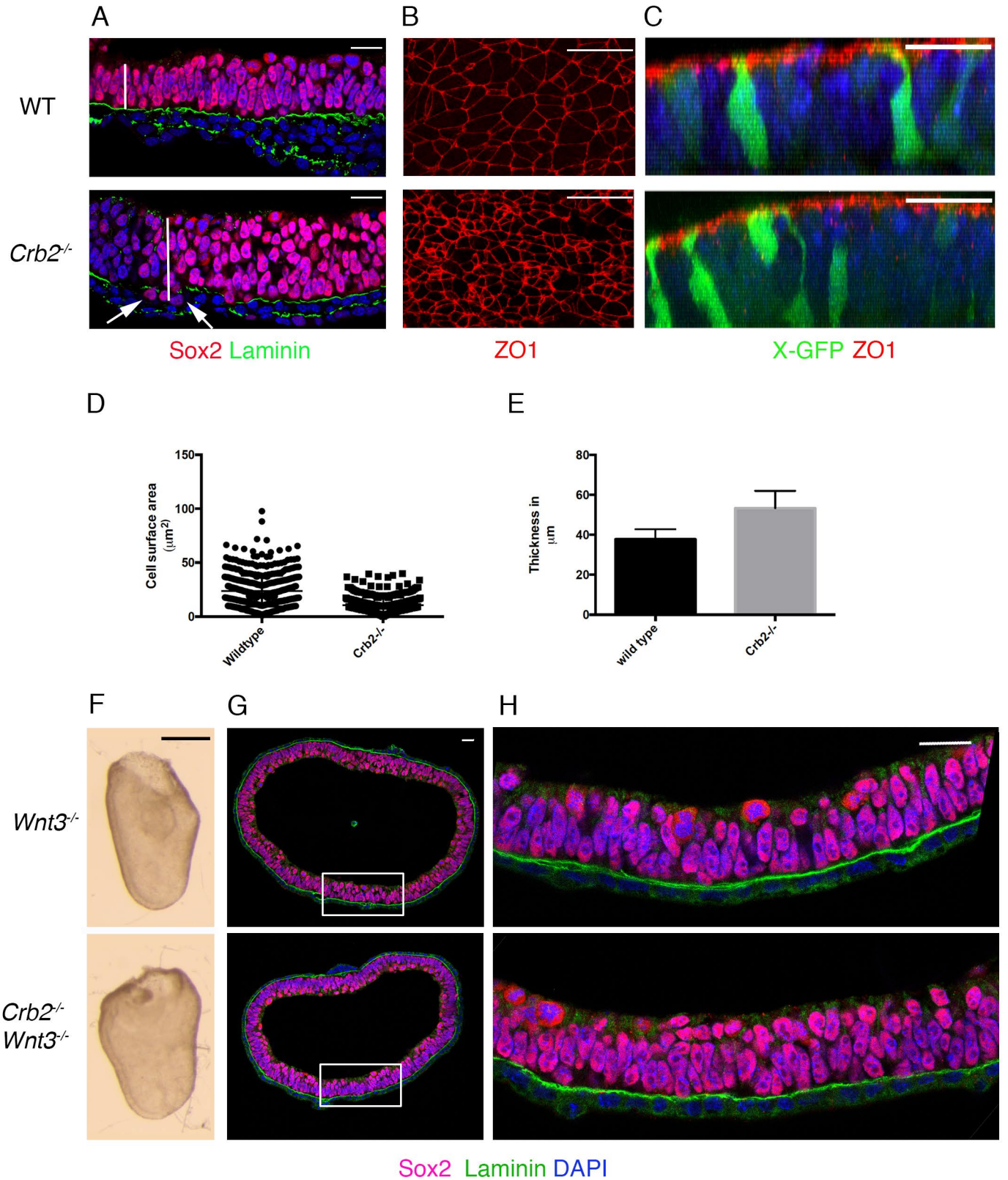
A
B
C
WT
Crb2-/-
Sox2 Laminin
ZO1
X-GFP ZO1
D
E
Cell surface area (μm2)
150
100
50
0
Wildtype
Crb2-/-
Thickness in μm
80
60
40
20
0
wild type
Crb2-/-
F
G
H
Wnt3-/-
Crb2-/- Wnt3-/-
Sox2 Laminin DAPI

Figure 8

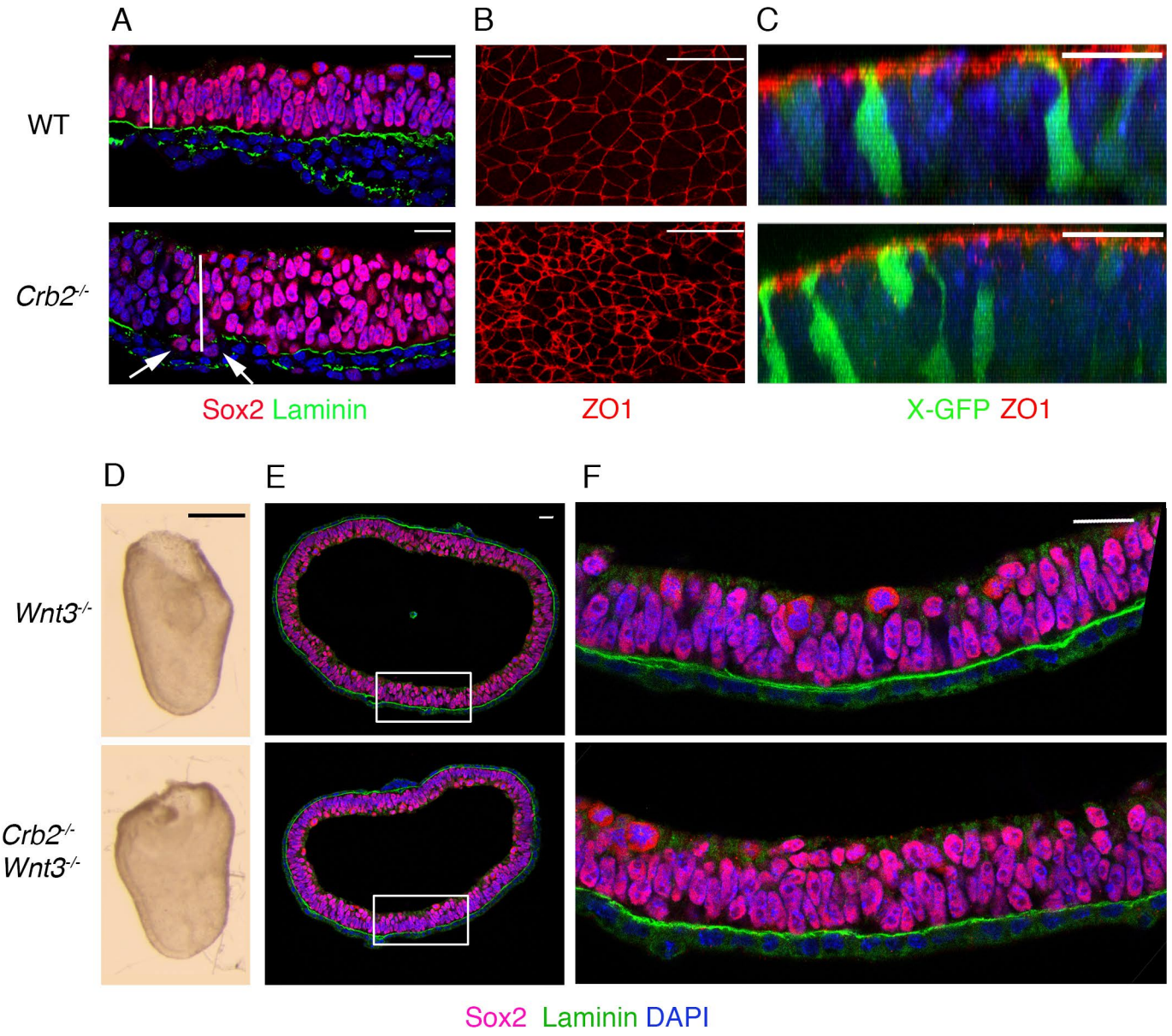
A
B
C
WT
Crb2-/-
Sox2 Laminin
ZO1
X-GFP ZO1
D
E
F
Wnt3-/-
Crb2-/-
Wnt3-/-
Sox2 Laminin DAPI

Methods

Mouse strains

The conditional allele of *Crumbs2* [ref. 42] was crossed to *CAG-Cre* (Jackson Laboratory) to generate the null allele (*Crumbs2*$^{-/-}$). *Crumbs3*$^{-/-}$ mice were re-derived from frozen embryos obtained from the Mutant Mouse Regional Resource Center. The conditional allele of *Wnt3* [ref. 43], *Crumbs1*^{rd8} [ref. 44], *X-linked GFP* [ref. 16], *GFP-GPI* [ref. 19], *Brachyury-Cre* [ref. 18], and *Sox2-Cre* [ref. 17] have been described. The *mT/mG* [ref. 45] and *EIIA-Cre* [ref. 46] mice were obtained from Jackson Laboratory. Male and female mice of 8-16 weeks old were used to generate embryos aged 6.5 dpc to 9.0 dpc used in this study. Most experiments were carried out in the FVB background, with the exception that the mT/mG *EIIA-Cre* experiments were in a mixed background after 1-2 generations of backcrossing to FVB. Analysis of *Crumbs2* mutants was in FVB background. All crosses with doubles mutants are in a mixed background. Animals were housed and bred under standard conditions in accordance with institutional IACUC guidelines. The MSKCC IACUC approved the experiments.

Phenotypic analysis

Whole mount in situ hybridization was performed as described[47]. Embryos were dissected in ice cold PBS-BSA and fixed in 4% PFA for one hour at room temperature for immunostaining or over-night at 4°C for in situ hybridization. The embryos were embedded in OCT (optimal cutting temperature) and cryosectioned at 10-12 µm thickness. Immunostaining on frozen sections was performed as described[47]. Briefly sections were washed 3 times for 10 mins each in PBS (until OCT was washed out), following which they were incubated in blocking buffer (1% Heat inactivated donkey or goat serum, 0.1% triton X-100 in1X PBS) for 1-2 hours. Primary antibodies were diluted in blocking buffer and incubated overnight at 4°C. The secondary antibodies were also diluted in blocking buffer and incubated for 1 hour at room temperature. Rhodamine-conjugated phalloidin at 10 U/ml and DAPI were included in the secondary incubation. For *en face* imaging of the primitive streak, embryos were dissected out of the Reichert's membrane, cut on their lateral sides and flattened with forceps in ice cold PBS-BSA before fixing in 4% PFA. Following immunostaining, the embryos were flat mounted in Vectashield or ProLong gold with the apical side of the streak facing the coverslip. The position of the streak was determined morphologically as the midpoint of the epithelium along with left-right axis, running from the node till the allantois, with a large population of apically constricted cells. In all *en face* images, the center streak is positioned

in the middle of the image, distal down. Immunostaining with Myosin IIB and phalloidin revealed a high concentration of puncta along the primitive streak region of the epithelium.

Antibodies

The following antibodies were used: anti-CRB2 was from Jane McGlade (Hospital for Sick Children, Toronto) and was used at 1:50 [ref. 48]. Anti-SNAI1 was a gift from Antonio García de Herreros (University of Pompeu Fabra, Barcelona) and was used at 1:100 [ref. 49]. Anti-PatJ was a gift from André Le Bivic (Institut de Biologie du Développement de Marseille) and was used at 1:200 (ref. 50). Commercially available antibodies used were: anti-Sox2 (Santa Cruz 1:100, sc-17320), anti-E-cadherin (Sigma 1:200, U3254), anti-laminin (Sigma 1:200, L-9393), anti-Myosin IIB heavy chain (Covance 1:400, PRB-445P; DSHB 1:50, CMII 23), anti-ZO1 (Invitrogen (Zymed) 1:200, 33-9100), anti-Par3 (Millipore (Upstate) 1:200, 07-330), anti-acetylated α-tubulin (Sigma 1:1000, T6793), anti-γ tubulin (Sigma 1:500, T6557), anti-pERM (Cell Signaling 1:100, 3141), anti-aPKC (BD Biosciences 1:100, 610208), anti-Brachyury (R&D 1:200, AF2085), anti-Arl13B (1:2000) (ref. 51), anti-pHH3 (Millipore (Upstate) 1:500, 06-570) and anti-β-catenin (BD Biosciences 1:200, 610154). Confocal microscopy was performed using a Leica-Inverted SP5 or Leica-Upright SP5 laser, point-scanning confocal microscope. Confocal datasets were analyzed using the Volocity software package (Improvision).

Scanning Electron Microscopy

E7.75 embryos dissected in ice cold PBS and were fixed with 2% PFA and 2.5% glutaraldehyde in 0.1M sodium cacodylate buffer. Following fixation, embryos were dissected further to expose the primitive streak in 0.1 M cacodylate buffer and dehydrated in ethanol[52]. Scanning electron microscopy was performed using a field emission microscope (Supra 25; Carl Zeiss), and images were acquired with SmartSEM (Carl Zeiss).

Chimeras

Mice carrying both *GPI-GFP* transgene[19] and a null allele of *Crumbs2* were generated. Blastocysts generated from intercrosses between these mice were harvested. ES cells were generated from GFP-positive blastocysts using the 2i+LIF method[53]. GFP-labeled wild-type and *Crumbs2* mutant ES cells were independently injected into wild-type blastocysts, which were implanted in pseudopregnant females. Embryos were harvested between E9.5 to E10.5 (equivalent to E8.5 to E9.5 normal development, as chimeras are delayed). A total of 40

chimeras were analyzed. Endogenous GFP was used for the identification of *Crumbs2* mutant cells in the chimera analysis.

Anterior epiblast quantification

Single cells were selected and their areas were determined using Volocity software. The width of the anterior epiblast (early neural epithelium) was also determined using Volocity. Average area of cells and width of the anterior epiblast was calculated using Prism and the student t-test was used for statistical analysis. The error bars indicate standard error.

Myosin IIB-CRB2 quantification and statistical analysis

Single optical sections from *en face* double immunostaining of the primitive streak from wild-type embryos were selected and the respective CRB2 and Myosin IIB channels were separated. The intensity for each channel was individually thresholded. With a line-width selection of 10 units, cell edges with high CRB2 (high CRB2 = top 10% of intensities) were selected in ImageJ and labeled as High CRB2. The intensity for CRB2 was measured in the channel for the edges selected. The selected edges were replicated in the Myosin IIB channel and the corresponding intensity of Myosin IIB was measured. For the same images, cell edges with high Myosin IIB (high MYO = top 10% of intensities) were selected and labeled as High Myosin and the Myosin IIB intensity was measured in that channel. All intensities were normalized with their respective mean. This selection was duplicated in the CRB2 channel and the corresponding intensity measured. For Myosin IIB intensity measurements, cell edges were outlined using the ZO1 or phalloidin channel, and the corresponding values for Myosin intensity were measured using Fiji. The values for CRB2 and Myosin IIB were compared with two-tailed student t-test and box plots were plotted using Stata.

Mouse embryo culture for live imaging and image analysis

Embryos were dissected with their yolk sac and ectoplacental cone intact in media maintained at 37°C (DMEM/F12 with 10% FBS). The embryos were positioned with the posterior side facing the objective into a hole created in a freshly prepared collagen matrix (BD Biosciences) on a glass bottom 35-mm Matek dish equilibrated with dissection media and rat serum. The embryos were cultured in rat serum and imaged for 4-6 hours with Z-stacks taken every 8-10 minutes on a Leica SP5 or SP8 confocal microscope equipped with

an incubation chamber maintained at 37°C and 5% CO2. The time-lapse movies were analyzed using Imaris and Metamorph software.

Quantitative morphometric measurements of different volumetric parameters were performed using Imaris (Bitplane Inc.). Time-lapse Z-stack images of each embryo acquired by using identical acquisition parameters were loaded into Imaris. 3D renderings of the samples allowed identification of the regions of interest (ROI). Then stacks were 3D cropped based on ROI. The 3D data were thresholded to the boundaries of the membrane-GFP expressing cells to create a visual boundary for each cell. Using the surface creation tool in Imaris, surfaces were put on the GFP boundaries. Using defined fluorescence intensity and size criteria the surfaces/builds were filtered. Builds of the multiple GFP-labeled cells fused into one surface were eliminated. Surfaces were manually separated using the cutting tool if the contact site between cells was minimal (about 1-3 mm). Every surface was tracked over time to confirm identity and accuracy of surface building for every cell. Volumetric data and relevant statistics were exported for analysis, allowing for volume determination. Parameters obtained were ellipticity, sphericity and volume. For Imaris analysis of the surface shape: Ellipticity, *e*, was defined using the lengths of the semi-principal axes *a*, *b* and *c*.

$$e_{prolate} = \frac{2a^2}{a^2+b^2} \cdot \left(1 - \frac{a^2+b^2}{2c^2}\right)$$

$e_{prolate}$ = prolate Ellipsoid

a = b < c it is a prolate Spheroid (cigar-shaped)

$$e_{oblate} = \frac{2b^2}{b^2+c^2} \cdot \left(1 - \frac{2a^2}{b^2+c^2}\right)$$

e_{oblate} = oblate Ellipsoid

a < b = c it is an oblate Spheroid (disk-shaped)

The data were plotted by using Prism (GraphPad Software Inc.) for statistical analysis. Unpaired student's *t*-test was used to determine the statistical significance of the differences between cell shapes.

For analysis of polygon distribution at the streak, cell edges were outlined using ImageJ. The number of cell edges with high CRB2 was manually counted for each cell outlined in ImageJ. The graphs were plotted using Prism.

Statistics and Reproducibility

For each experiment 3-15 embryo samples were analyzed. Immunostaining experiments were repeated a minimum of three independent times to ensure reproducibility. All samples if preserved and properly processed were included in the analysis. No samples or animals were excluded. No statistical method was used to predetermine sample size. The experiments were not randomized. The Investigators were not blinded to allocation during experiments and outcome assessment.

Data availability

All data supporting the findings of this study are available from the corresponding author upon reasonable request.